Chemistry–A European Journal
Research Article
doi.org/10.1002/chem.202400798
Chemistry Europe
European Chemical Societies Publishing
www.chemeurj.org

# Classification and Identification of Perfume Scents by an Enantioselective Colorimetric Sensor Array of Chiral Metal-Organic-Framework-Based Fabry-Pérot Films

Kuo Zhan,[a, b] Anemar Bruno Kanj,[a] and Lars Heinke*[a]

Many odors, like perfumes, are complex mixtures of chiral and achiral molecules where the cost-efficient (enantio−)selective sensing represents a major technical challenge. Here, we present a colorimetric sensor array of surface-mounted metal-organic-framework (SURMOF) films in Fabry-Pérot (FP) cavities. The optical properties of the FP-SURMOF films with different chiral and achiral structures are affected by the (enantio−)selective adsorption of the analytes in the SURMOF pores, resulting in different responses to the analyte molecules. The read-out of the sensor array is performed by the digital camera of a common smartphone, where the RGB values are determined. By analyzing the sensor array data with simple machine learning algorithms, the analytes are discriminated. After demonstrating the enantioselective response for a pair of pure chiral odor molecules, we apply the sensor array to detect and discriminate a large number (16) of common commercial perfumes and eau de toilettes. While our untrained human nose is not able to discriminate all perfumes, the presented colorimetric sensor array can classify all perfumes with great classification accuracy. Moreover, the sensor array was used to identify unlabeled samples correctly. We foresee such an FP-chiral-SURMOF-based sensor array as a powerful approach toward inexpensive selective odors sensing applications.

## Introduction

Chiral molecules are widely used in various perfume products.[1] Many chiral odor molecules possess an enantioselective scent, where the odor of different isomers is perceived differently by the human olfactory system, i.e. our nose. For example, the odor of *R*-2-octanol (*R*-OcOH) is described as creamy, cucumber, fatty and sour, while the odor of *S*-2-octanol (*S*-OcOH) has more of a mushroom odor.[1c] The human olfactory system contains about 400 olfactory receptors, capable of binding with different chiral odor molecules and generating recognition patterns in the olfactory part of the neural system.[2] Consequently, most chiral odors can be easily characterized by a panel of judges with "trained noses". However, if the trained noses inhale a large number of odor molecules in a short period of time, it leads to neural fatigue and decreases the accuracy of discerning the odors by the sense of smell.[2b,3] In addition, while trained human noses can discriminate a large number of odors, untrained noses are less powerful. Therefore, an enantioselective, reversible and repeatable sensor system (or sensor array) holds the potential for various enantioselective discrimination applications. To this aim, in recent years, various groups have presented simple optical sensor arrays allowing the enantioselective discrimination of the isomers of a chiral molecule and their isomer mixtures.[4]

A Fabry-Pérot (FP) cavity is an optical interferometric structure consisting of two reflectors separated by a thin film.[5] It has gained significant attention in the field of chemical sensing because its optical properties are directly affected by the refractive index (RI) that, in the case of porous materials, can be sensitive to the environment.[6] By monitoring the changes in the reflection spectrum, or more conveniently, by monitoring the color of the FP film resulting from the reversible adsorption/desorption of guest molecules in the inner film, it becomes feasible to accurately and readily detect the targeted analytes.[7]

To make FP-film-based optical sensors, transparent and porous materials are required. Thin films of metal-organic frameworks (MOFs), composed of metal nodes connected by organic ligands, are ideally suited for such tasks.[8] MOFs exhibit unique properties such as high surface areas, diverse structures and tunable functionalities, making them well-suited for applications in sensors. Thin and homogenous films can be prepared in a layer-by-layer fashion, resulting in surface-mounted MOF (SURMOF) films.[9] In a previous study, we used an FP-SURMOF-sensor array for the classification of a large amount of different volatile organic compounds (VOCs) and to classify food degradation.[10]

[a] Dr. K. Zhan, Dr. A. B. Kanj, Priv.-Doz. Dr. L. Heinke
Institute of Functional Interfaces (IFG)
Karlsruhe Institute of Technology (KIT)
Hermann-von-Helmholtz-Platz 1, 76344, Eggenstein-Leopoldshafen, Germany
E-mail: Lars.Heinke@kit.edu

[b] Dr. K. Zhan
School of Physical Science and Engineering
Beijing Jiaotong University
100044, Beijing, China

Supporting information for this article is available on the WWW under https://doi.org/10.1002/chem.202400798

Here, we present a chiral colorimetric sensor array based on homochiral and achiral FP-SURMOF films for the detection, classification and identification of perfume odors. This sensor array is made of SURMOFs with different structures, which are homochiral SURMOFs of type $Cu_2(DCam)_2(dabco)$[11] and $Cu_2(DCam)_2(Bipy)$[11] and achiral SURMOF of type HKUST-1.[12] (DCam stands for chiral (1*R*,3*S*)-(+)-camphoric acid as layer linker, dabco for 1,4-diazabicyclo[2.2.2]octane and BiPy for 4,4′-bipyridine as pillar linkers, HKUST-1 for Hong Kong University of Science and Technology.) First, this sensor array was tested with a pair of pure chiral test odors, which is *R*/*S*-2-octanol (*R*/*S*-OcOH), at low concentrations (0–50 ppm) using UV-vis spectroscopy, demonstrating its enantioselective properties. Additionally, the digital camera of a common smartphone (iPhone XR) was used to determine the color of the optical sensor. By using the RGB values and simple machine learning algorithms, like k-Nearest Neighbor (k-NN), the analytes were classified with 99% accuracy. Based on this, we applied this enantioselective colorimetric sensor array with the simple and cost-efficient read-out (by the smartphone camera) for the classification and identification of 16 commercial perfumes, reaching a similar high accuracy. Moreover, unlabeled samples (randomly taken from the 16 perfumes) were correctly identified by the sensor system. We like to stress that we (with our untrained human nose) were not able to do this. To the best of our knowledge, such a study has not yet been presented to date, pushing the application of functional, nanoporous-materials-based sensors.

## Results and Discussion

The FP-SURMOF films were prepared in a layer-by-layer fashion on the reflecting substrate. The top-mirror of the FP-cavity was deposited by sputtering Pt on the SURMOF films. The crystallinity of the SURMOF films with different structures was explored by X-ray diffraction (XRD). The XRD data show that all films have crystalline structures which correspond to the targeted SURMOFs, Figure 1. The crystallinities of the samples are not affected by the sensing experiments, Figure S9. The samples are further characterized by infrared reflection absorption spectroscopy (IRRAS, supporting information, Figure S2), verifying the composition of the SURMOF structures. The SEM images, see Figure 1, show that the FP-SURMOF films have a homogeneous morphology with a thickness of 0.3–0.5 μm. The CD spectra of the SURMOF films are shown in Figure S11, indicating the homochiral character of $Cu_2(DCam)_2(dabco)$ and $Cu_2(DCam)_2(BiPy)$ as well as the achiral character of HKUST-1.

First, the FP-SURMOF sensor array was tested for a pair of chiral odors, *R*- and *S*-2-octanol (*R*/*S*-OcOH), as analytes. Initially, for exploring the enantioselective response and for exploring the spectral changes, UV-vis spectroscopy was used for the sensor-read-out of the colorimetric sensors. The reflectance spectra of the FP-SURMOF films, pristine and exposed to the saturated chiral test odors (*R*-/*S*-OcOH), are shown in Figure 2a (and in Figures S4 and S5). The spectra show photonic patterns with peaks at approximately 500 nm which shift to larger wavelengths upon analyte exposure. The reflectance spectra of

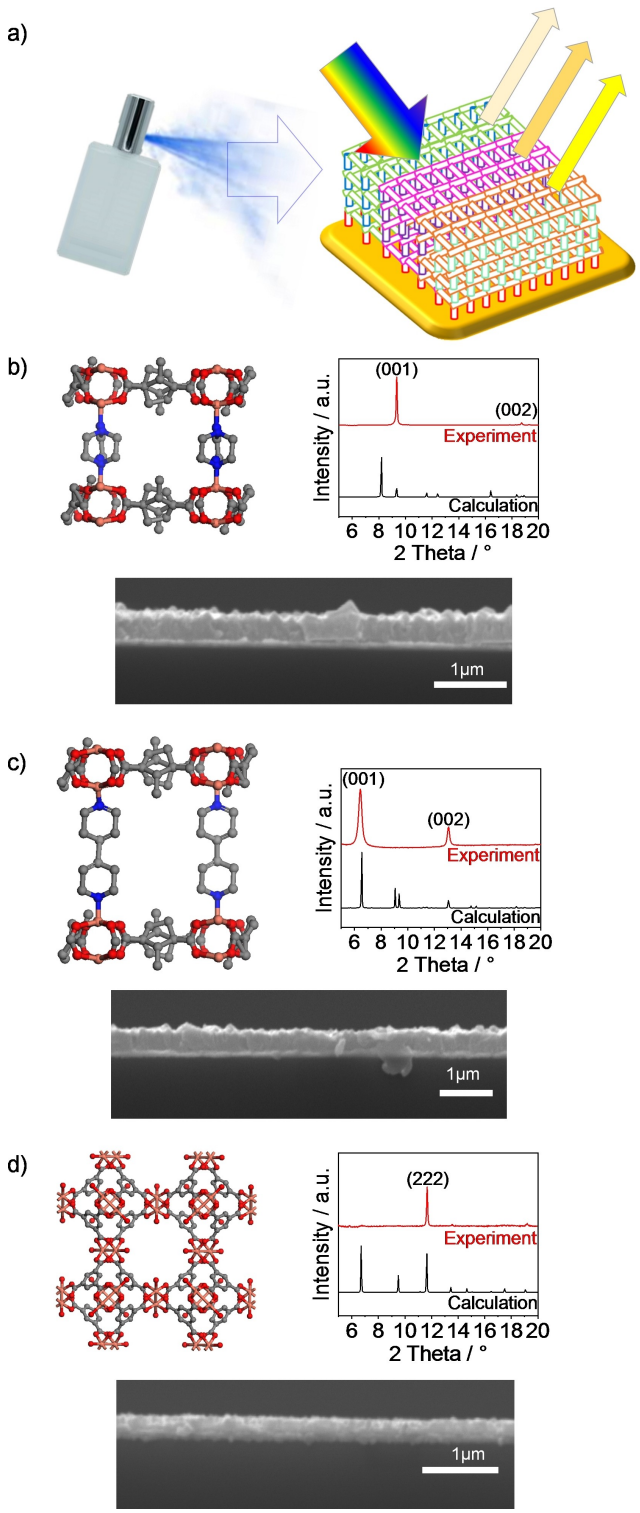


**Figure 1. a)** Sketch of FP-SURMOF films, where the incident light is selectively reflected. The three different MOF films as well as the perfume odors are sketched. Sketches of the SURMOF structures of **b)** $Cu_2(DCam)_2(dabco)$, **c)** $Cu_2(DCam)_2(Bipy)$ and **d)** HKUST-1. The color code of the atoms is: C grey, O red, Cu orange and N blue. H is not shown. (Another presentation of the chemical structures is shown in Figure S1.) The X-ray diffractograms of the SURMOF samples (red) with the calculated XRD as reference (black) are shown next to the respective SURMOFs. The X-ray wavelength is 0.154 nm. The experimentally observed peaks are labeled. The SEM images of the broken samples, showing the cross-sections, are shown below.

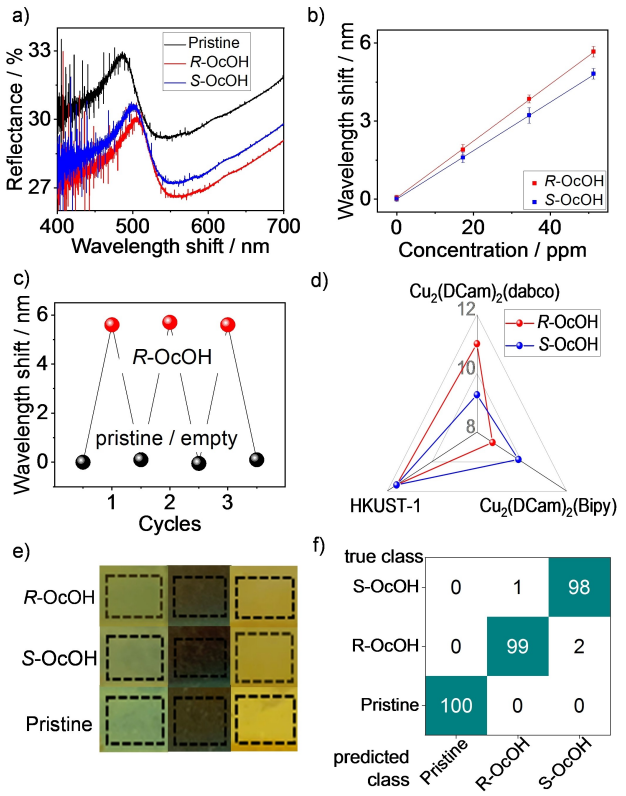


**Figure 2. a)** The reflectance spectra of the FP-$Cu_2(DCam)_2$(dabco) film in the atmosphere of saturated chiral odors, see labels (the same color code is used in all panels). **b)** The wavelength shift of the reflectance peak of the FP-$Cu_2(DCam)_2$(dabco) film *versus* analyte concentration. The UV-vis reflectance spectra as well as the intensity changes of the reflectance peak for the FP-SURMOF films are shown in Figure S3–S5. **c)** The wavelength shift of the FP-$Cu_2(DCam)_2$(dabco) film for ≈50 ppm *R*-OcOH, testing the reversibility and repeatability. **d)** Radar plot of the wavelength sensitivity (see panel b) of the sensors. The units of the axes are $10^{-2}$ nm/ppm. **e)** Photos of the sensor array, either in pure nitrogen (pristine) or in saturated *R*/*S*-OcOH vapor, see labels. (The dotted rectangles with a size of 2 mm x 3 mm present the area where the RGB values were determined.) Right: FP-$Cu_2(BDC)_2$(dabco) film, center: FP-$Cu_2(BDC)_2$(Bipy) film, left: FP-HKUST-1 film. **f)** The k-NN confusion matrix of the RGB data from the sensor array (measured by the smartphone) in saturated *R*/*S*-OcOH vapors. Correct classifications are shown on the main diagonal of the matrix; misclassifications are the other values. The numbers are in percent.

the FP-$Cu_2(DCam)_2$(dabco), FP-$Cu_2(DCam)_2$(Bipy) and FP-HKUST-1 films in a controlled atmosphere with small analyte concentrations (0–50 ppm) are shown in Figures S3, S4 and S5. The shifts of the reflectance peaks and of the intensities of the FP-SURMOF films are presented in Figure 2b, S3, S4 and S5. In the range of 0–50 ppm, the FP-films show linear dependences of the reflectance peak shift *versus* concentration. The slopes of the wavelength shift *versus* concentration (Figure 2b, S4, S5) are regarded as the wavelength sensitivity. The wavelength sensitivities are in the range of 0.08 to 0.12 nm ppm$^{-1}$. Remarkably, the sensitivities of the different enantiomers are different in the chiral SURMOFs (*R vs. S*: 0.11 nm ppm$^{-1}$ *vs.* 0.09 nm ppm$^{-1}$ for FP-$Cu_2(DCam)_2$(dabco) and 0.087 nm ppm$^{-1}$ *vs.* 0.099 nm ppm$^{-1}$ for FP-$Cu_2(DCam)_2$(BiPy)), showing the enantioselective response of the sensor array. Please note, the opposing adsorption preference of *R*-OcOH and *S*-OcOH in $Cu_2(DCam)_2$(dabco) *versus* $Cu_2(DCam)_2$(BiPy) was also found in a previous gravimetric study.[13] As expected, in contrast to the chiral SURMOFs, the achiral SURMOF shows no enantioselectivity.

The slope of the intensity changes *versus* concentration (Figures S3, S4 and S5) is regarded as the intensity sensitivity. The intensity sensitivities are in the range of −0.02 to −0.03 % ppm$^{-1}$, Table S1.

From the sensitivities, the corresponding limits of detection (LOD: wavelength-LOD, Intensity-LOD) can be calculated, Table S1. The determined LODs are in the range of 1 ppm to 3 ppm, depending on the MOF sensor and the analyte.

The reversibility and repeatability of the FP-SURMOF films are demonstrated by repeating the exposure to ≈50 ppm *R*-OcOH vapor, Figure 2c. The data show that the sensor exposure is fully reversible and repeatable, as a result from the reversible absorption and desorption of *R*-OcOH in the SURMOF pores.

The wavelength-sensitivity radar plot of the FP-SURMOF sensor array is shown Figure 2d. The chiral films, i.e. $Cu_2(DCam)_2$(dabco) and $Cu_2(DCam)_2$(Bipy), show different wavelength sensitivities for the different enantiomers, and the achiral FP-HKUST-1 film shows the same wavelength sensitivity for both enantiomers. As result, the radar plot (Figure 2d) presents a unique characteristic pattern or fingerprint for each analyte (*R*/*S*-OcOH), which allows its enantioselective qualitative discrimination. Briefly, the different sensitivities of the FP-SURMOF films depend on the different adsorption properties of the enantiomer in the FP-SURMOF films. Upon exposure to the analyte atmospheres, the selective analyte adsorption causes the different RI changes of the SURMOF films, showing a corresponding specific optical response. More details of the sensing principle are given in the SI.

To investigate the accuracy of discriminating the pair of chiral odors (*R*-/*S*-OcOH) by UV-vis spectroscopy, we analyzed the reflectance spectra data with a simple machine learning algorithm, here, k-Nearest Neighbor (k-NN). The accuracies of the data classification are shown in the confusion matrix, Figure S6. It shows the quantitative discriminations of the chiral test odors (*R*/*S*-OcOH) at different concentrations by k-NN. It indicates a correct identification with perfect classification accuracy of 100 %.

The analyte exposure to the FP-SURMOF sensors exhibit substantial wavelength shifts of the reflectance peaks, consequently the colors of the FP films changes. To take advantage of the color change, we used a very simple and inexpensive way for the read-out of the sensor data. We placed the FP-SURMOF sensors next to each other and took photos of the sensor array with the digital camera of a common smartphone (here we use an iPhone XR). From the pictures (without color balance), the RGB values were used as the sensor signal. The RGB data were also analyzed by k-NN to recognize and classify the chiral molecules. Figure 2e shows the photos of the FP-SURMOF films in different analyte atmospheres, exhibiting color changes of the sensors as colorimetric response. The RGB values of the sensor array are shown in Table S2. The k-NN result of the RGB colorimetric response of the sensor array of different chiral odors is shown in Figure 2f. The average classification

accuracy by using the k-NN algorithm is 99.0% for the saturated chiral odors (*R*/*S*-OcOH). This value is slightly smaller than the classification accuracy by using the UV-vis spectra (100%). However, it is still large enough to precisely determine each chiral odor. The outcomes reveal remarkably high classification accuracies, demonstrating the capability of the FP-SURMOF sensor array to perform enantioselective classification of chiral odor molecules with this simple and omnipresent analysis technique (smartphone), avoiding expensive lab equipment.

In addition to 2-octanol, an enantioselective adsorption behavior in $Cu_2(DCam)_2(dabco)$ SURMOFs was also previously found for limonene, 1-phenylethylamine and 1-phenylethanol.[13] Thus, we believe the sensor system can be applied to many chiral molecules and mixtures.

As final aim of this study, we use the FP-SURMOF sensor array with the smartphone camera as a selective colorimetric sensor system for practical applications. We conduct the discrimination sensing tests for 16 commercial perfumes, see Table 1. Such perfumes typically contain mixtures of ethanol, water and various (chiral and achiral) odor molecules, such as coumarin, vanillin, citronellal, *R*-/*S*-linalool, *R*-/*S*-limonene, *R*-/*S*-1-phenylethanol, *R*/*S*-2-octanol and many more.[1b,14] (For the used samples, see table 1, we were unable to determine the molecular components and their mixture.) The perfumes are classified by exposing the sensor array to their vapor and taking pictures with the smartphone. Figure 3a (and Figure S7) shows pictures of the sensor array in different perfume vapors. The determined RGB values, Table S3, change significantly. For example, while the RGB values for the pristine FP-$Cu_2(DCam)_2(dabco)$ film is (116,148,93), the RGB values are (102,128,72) for perfume #1, (95,119,65) for perfume #6, (127,130,61) for perfume #11.

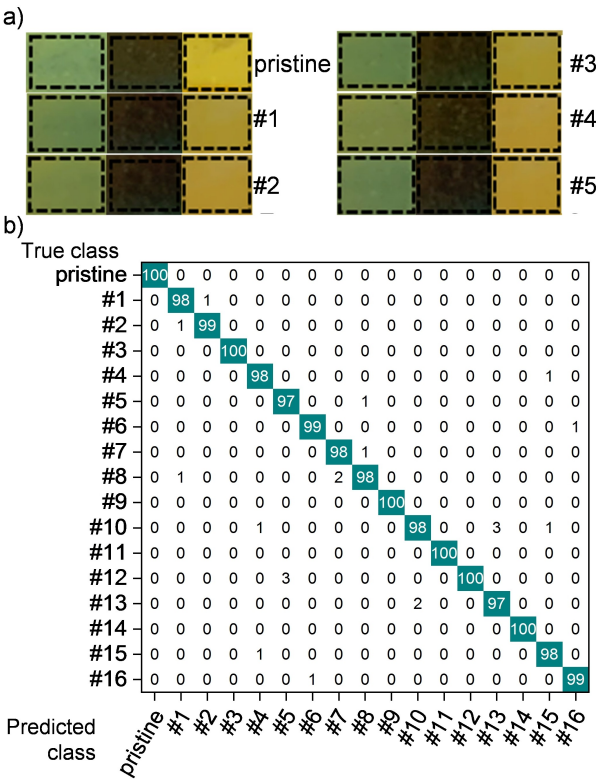


**Figure 3. a)** Photos of the sensor array in pure nitrogen (pristine) and in the vapor of perfumes #1–#5, see labels. Left: FP-$Cu_2(DCam)_2(dabco)$, Center: FP-$Cu_2(DCam)_2(BiPy)$, Right: FP-HKUST-1. The dotted rectangles with a size of 2 mm x 3 mm represent the area where the RGB values were determined. More pictures (from all samples) are given in Figure S7. **b)** The k-NN confusion matrix of the sensor data of the FP-SURMOF array in the vapor of the 16 perfumes and the pristine sample. The numbers are in percent.

**Table 1.** The explored samples, which are popular commercial perfumes, eau de toilettes and after shaves.

| Number | Name of perfume, eau de toilette or after shave |
|---|---|
| #1 | Eau de Toilette Jasmine – L'Occitane (for women) |
| #2 | Thé Noir 29, Eau de Perfum, Le Labo (for women) |
| #3 | Eternity for Men, Calvin Klein, Cologne (for men) |
| #4 | Alive – Boss, Perfume (for women) |
| #5 | Kaifragrance.com (for women) |
| #6 | Pure Grace (for women) |
| #7 | Mexx Perspective (for men) |
| #8 | Gammon – Cool Action, Aftershave (for men) |
| #9 | Hugo Boss, After Shave (for men) |
| #10 | Plumeria (Roller, Hawaii) (for women) |
| #11 | Forever Floralis (for women) |
| #12 | Lancome Miracle Forever (for women) |
| #13 | Thierry Mugler – Angel Muse – Eau de Parfum (for women) |
| #14 | BB Bruno Banani – Not For Everybody – Made For Men, Eau de Toilette (for men) |
| #15 | Bruno Banani – Not For Everybody (for men) |
| #16 | Dior J'adore, Deodorant Parfum (for women) |

Figure 3b shows the k-NN confusion matrix based on the RGB data analysis of the sensor array in the vapor of the 16 perfumes. The data indicate a clear discrimination of all perfumes with a high classification accuracy of 98.9%. This demonstrates that the presented colorimetric sensor array is able to classify a large number of odor samples by using a common smartphone for analysis, avoiding expensive lab equipment.

We like to stress that, while we were able to distinguish and recognize some perfume samples by smelling (i.e. with our "untrained" olfactory system), we were not able to classify all samples by smelling.

In addition to the kNN analysis, the sensor data were analyzed by Principal Component Analysis (PCA) and Linear Discriminant Analysis (LDA). The 2-dimensional (2D) PCA plot (where the 9-dimensional sensor data were reduced to 2 dimensions) is shown in Figure 4. The plot visualizes that the signals of the different perfumes can be clearly discriminated. The corresponding LDA plot is shown in Figure S8.

Based on the superior classification performance, we explore whether the sensor system can be used to identify "unlabeled" samples. (Here, "unlabeled" means that the samples were taken from the 16 perfumes, but it was not labeled which samples they were. This was unknown to the experimentalist.)

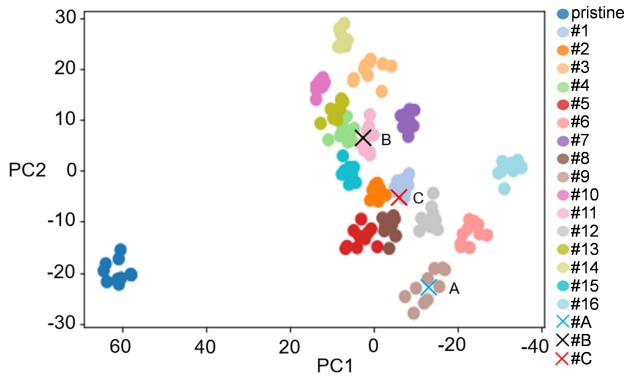


**Figure 4.** 2D-plot of the PCA results of the sensor array for the 16 perfume samples (see labels) and for the prediction of 3 unlabeled perfumes.

To this aim, 3 unlabeled perfumes (#A, #B and #C) were used as analyte samples, their RGB values of the sensor array were determined and the data were analyzed by PCA. Their sensor responses are shown in Figure 4. By comparing the position of the unlabeled samples on the 2D PCA plot, clear matches can be identified. The signal of unlabeled perfume #A matches the signals of perfume #9, unlabeled perfume #B matches the signals of perfume #11 and unlabeled perfume #C matches the signals of perfume #1. All of these assignments were correct. This indicates a very high recognition capability of the perfumes by the sensor array. It also shows that it could be used for practical sensing applications, e.g. to identify different (potentially counterfeit) perfumes.

## Conclusions

A small and portable sensor array of nanoporous chiral SURMOF Fabry-Pérot films is used for the reversible and repeatable enantioselective optical classification and identification of a large number of perfumes by their vapor. Herein, the Fabry-Pérot-sensor array is based on homochiral SURMOFs ($Cu_2$(DCam)$_2$(dabco) and $Cu_2$(DCam)$_2$(Bipy)) and an achiral SURMOF (HKUST-1). In addition to its enantioselective sensing property demonstrated by the UV-vis reflection spectra analysis, the digital camera of a common smartphone was used to quantify the color changes of the colorimetric sensor array. The sensor array shows high sensitivities and low LODs in the range of 1–3 ppm for odor molecules of type *R*-/*S*-2-octanol with a very high enantioselectivity, reversibility and repeatability. Particularly, combined with a common smartphone, the sensing system represents a simple and very inexpensive device. That way, the colorimetric sensor array was used to discriminate 16 representatives of commercial perfumes with a high accuracy (99%), using k-NN for the data classification. In addition, unlabeled perfume samples were correctly identified with the sensor array by using PCA and LDA analysis.

The study demonstrates that such simple and low-cost sensor systems can be used to discriminate and identify large numbers of complex odor samples. We foresee that various functional, chiral or achiral, SURMOF structures can be implemented in such FP-SURMOF-based colorimetric sensor systems, allowing the reliable discrimination of even more complex odor samples and mixtures and/or of larger numbers of perfumes. We believe it might find application in identifying counterfeit and diluted perfumes, aromas, flavors and other odors. While the layer-by-layer synthesis approach enables the scale-up to large areas for certain SURMOF structures,[15] enhancing the large-scale synthesis of homochiral pillared-layer SURMOF films as well as improving the cost-efficiency with respect to the substrate and top-mirror coating are necessary before advancing towards practical real-world applications.

## Methods

The chiral SURMOF films with different structures were prepared in a layer-by-layer fashion.[11,13] The substrates (gold-coated silicon wafer) were alternatively immersed in the ethanolic solutions of the metal nodes and of the linker molecules, see supporting information (SI) Figure S1. The metal nodes are $Cu(CH_3COO)_2{\cdot}H_2O$ with a concentration of 0.2 mM. The linker molecules are DCam and dabco (for $Cu_2$(DCam)$_2$(dabco)), DCam and Bipy (for $Cu_2$(DCam)$_2$(Bipy)) and trimesic acid (BTC) (for HKUST-1) with a concentration of 0.1 mM each. The syntheses were performed with a dipping robot with 180 cycles. To enhance the optical quality of the SURMOF films, the samples were exposed to ultrasonication during the ethanol cleaning step every 5 cycles.[16] The FP-top mirrors, i.e. the platinum films of about 5 nm thickness, were sputtered on top of the SURMOF films by a Sputter Coater MED020. The Pt film acts as a top mirror, the Au substrate act as a bottle mirror and the SURMOF thin film act as the inner film, resulting in the FP-SURMOF film.

The X-ray diffraction (XRD) analysis was performed with a Bruker D8-Advance diffractometer with a Bragg-Brentano (θ-θ) geometry (also referred to as out-of-plane) and a Cu-anode with a radiation wavelength of $\lambda = 0.154$ nm. The (111) peak of the gold substrate was used as a reference, verifying the correct sample height.

UV-vis reflectance spectra were recorded with an Agilent Cary 5000 spectrometer and UMA unit.

A Fourier transform infrared reflection absorption spectrometer (IRRAS) Bruker Vertex 80 was used for the vibrational spectroscopy of the samples. The spectra were recorded in grazing incidence reflection mode at an angle of incidence of 80° relative to the surface normal using a liquid nitrogen-cooled mercury–cadmium–telluride mid-band detector.

The CD spectra of the SURMOF samples on quartz glass substrates were measured using a Jasco J-1500 spectropolarimeter at room temperature. A blank quartz substrate was used for the background correction. The spectra were recorded from 600 to 200 nm in 1-nm-steps using a 100 nm min$^{-1}$ scan speed. Each spectrum is the result of the accumulation of three spectra. The samples were positioned perpendicular to the incident light beam on a rotating stage. To reduce artifacts (due to linear dichroism or birefringence caused by imperfections in the sample, such as slight vertical misalignment of the substrates or strain in the quartz glass plates), the spectra were recorded at 8 angles and then averaged.

Scanning electron microscope (SEM) images were recorded with a TESCAN VEGA3 tungsten heated filament SEM. To avoid charging effects, the samples were coated with a thin Au/Pd film. The samples were imaged under high vacuum conditions and using an acceleration voltage of 15 kV.

For the sensing experiments, first the analyte vapors were detected using an Agilent Cary 5000 UV-vis spectrometer at room temperature and the FP-SURMOF film samples are located in a cuvette with a gas in/out tube system (for Figure 2). The wavelength resolution was set to 0.1 nm. The spectra were recorded in reflectance with an angle of 30° to the surface normal. The position of the reflectance peak wavelength was determined by fitting a Gaussian function to the data in a range of about 20 nm. The pristine samples were stored in a pure nitrogen atmosphere. The adsorption step for the sensing test was 1 h, the desorption (for the release of the analytes) was 2 h to ensure that all guest molecules were desorbed and the samples returned to their pristine state. The intensity of the reflectance peak (in a range of 5 nm around the reflectance peak maximum) was used as a sensor response for the kNN analysis. Two mass flow controllers (MFCs) controlled the gas flow inside the cuvette. The gas stream of the carrier gas (nitrogen) was divided into 2 streams, one stream provides a constant nitrogen flow of 300 ml $min^{-1}$. The other stream passes through the analyte-filled wash bottle to produce an analyte-enriched vapor stream. Both gas streams were combined with fixed flow rates, controlling the partial pressure in the final gas stream. 2-octanol has a vapor pressure of 20.7 Pa at 20 °C.[17] The *R-/S*-octanol-enriched gas flow and the pure nitrogen flow were merged 1:3, 1:5 and 1:11, resulting in a octanol concentration of ≈52 ppm, ≈34 ppm and ≈17 ppm.

The photos of the sensors for the colorimetric response analysis are taken by a common smartphone. The sensors were placed next to each other in a sealed transparent Petri dish with a gas flow going in and out (via tubes). An iPhone XR, fixed at a distance of 40 cm, was used to take the photos.

For the analysis of the UV-vis data for the *R-/S*-OcOH sensing, the data analysis and classification were performed using standard k-nearest neighbor (k-NN) as well as Principal Component Analysis (PCA) and Linear Discriminant Analysis (LDA) for evaluating the possibility of clustering. The machine learning algorithms via program codes written in Python 3 in the open-source platform Jupyter Notebook were used. For the k-NN, a total of 50 data points of the reflectance intensity values at the reflectance peak (5 nm around the reflectance peaks at ~478 nm for $Cu_2(DCam)_2$(dabco), ~488 nm for $Cu_2(DCam)_2$(Bipy), ~565 nm for HKUST-1 with a resolution of 0.1 nm) were collected before and after the analyte exposure. Each data point for the analysis includes the reflectance intensities of the FP-SURMOF films, thus each data point is a 3-dimensional vector. A total of 150 data points for analysis were collected for the pristine sample and the 2 analytes (i.e. *R/S*-2-octanol). The K value in k-NN was set to 12 (which is close to the square root of 150).

For the analysis of the data from the phone camera, 10 consecutive pictures were used and the RGB values were determined. For the k-NN, PCA and LDA analysis of the RGB data, a total of 10 data points of the RGB values of the photos were collected before and after the vapor exposure. Each data point includes the three RGB values of the 3 FP-chiral-MOF-film, thus each data point is a 9-dimensional vector. A total of 270, 1530 and 1800 data points for the analysis were collected from the pristine sample and the 2 chiral odors, the 16 perfumes and the 16 perfumes with 3 unlabeled perfumes, respectively. The K value in k-NN was set to 16, 39 and 42, respectively (which is close to the square root of 250, 1530 and 1800). The data were classified using 5-fold cross-validation, where 80% of the data points were used as the training set and 20% were used as the test set. The outcome of the k-NN algorithm is the grouping of the data into different classes and comparing the assignments to the correct or wrong classes, shown in the confusion matrix. The outcome of the PCA and LDA are (after dimensionality reduction) the 2D plots, allowing the visual grouping of the data. For the dimensionality reduction in PCA, we calculated the 9-dimensional vector data's covariance matrix and its corresponding eigenvalues, the largest 2 eigenvalues are selected along with their corresponding eigenvectors to form a new matrix. We then projected our 9-dimensional original data onto this new matrix, using these 2 eigenvectors as the axes in the final 2D plot to reduce the 9-dimensional vector data to 2 dimensions. See also ref. [18]. For the dimensionality reduction in LDA, we calculated the 9-dimensional vector data's between-class scatter matrix $\omega_1$ and within-class scatter matrix $\omega_2$, the largest 2 eigenvalues and their corresponding eigenvectors of the $\omega_1^{-1}\omega_2$ are selected as the new matrix. We then projected the 9-dimensional original data onto this new matrix, using these 2 eigenvectors as the axes in the final 2D plot to reduce the 9-dimensional vector data to 2 dimensions. See also ref. [18]. The used program codes (based on the previous codes in ref. [19]) are given in the SI.

## Acknowledgements

We thank Yunzhe Jiang (KIT) for support with the SEM measurements and the Pt sputtering. The authors acknowledge financial support by the Deutsche Forschungsgemeinschaft (DFG, via HE 7036/5-2), the Chinese Fundamental Research Funds for the Central Universities 20211YJS175 and the China Scholarship Council (CSC). Open Access funding enabled and organized by Projekt DEAL.

## Conflict of Interests

The authors declare no conflict of interest.

## Data Availability Statement

The data that support the findings of this study are available from the corresponding author upon reasonable request.

**Keywords:** metal-organic frameworks · optical sensor · enantioselective · perfumes

[1] a) R. Bentley, *Chem. Rev.* **2006**, *106*, 4099–4112; b) B. Schilling, R. Kaiser, A. Natsch, M. Gautschi, *Chemoecology* **2010**, *20*, 135–147; c) E. Brenna, C. Fuganti, S. Serra, *Tetrahedron: Asymmetry* **2003**, *14*, 1–42.
[2] a) C. Trimmer, A. Keller, N. R. Murphy, L. L. Snyder, J. R. Willer, M. H. Nagai, N. Katsanis, L. B. Vosshall, H. Matsunami, J. D. Mainland, *Proc. Natl. Acad. Sci. USA* **2019**, *116*, 9475–9480; b) J. D. Mainland, Y. R. Li, T. Zhou, W. L. L. Liu, H. Matsunami, *Sci. Data* **2015**, *2*, 1–9.
[3] M. Son, J. Y. Lee, H. J. Ko, T. H. Park, *Trends Biotechnol.* **2017**, *35*, 301–307.
[4] a) M. J. Cich, I. M. Hill, A. D. Lackner, R. J. Martinez, T. C. Ruthenburg, Y. Takeshita, A. J. Young, S. M. Drew, C. E. Buss, K. R. Mann, *Sens. Actuators B* **2010**, *149*, 199–204; b) H. Iida, M. Miki, S. Iwahana, E. Yashima, *Chem. Eur. J.* **2014**, *20*, 4257–4262; c) R. Bhushan, *Chemistry-an Asian Journal* **2023**, *18*, e20230082.
[5] T. K. Gangopadhyay, S. Mandal, K. Dasgupta, T. K. Basak, S. K. Ghosh, *Appl. Opt.* **2005**, *44*, 3192–3196.
[6] M. R. Islam, M. M. Ali, M.-H. Lai, K.-S. Lim, H. Ahmad, *Sensors* **2014**, *14*, 7451–7488.
[7] a) S. Khan, S. Le Calvé, D. Newport, *Sens. Actuators A Phys.* **2020**, *302*, 111782; b) R. Kanawade, A. Kumar, D. Pawar, D. Late, S. Mondal, R. K. Sinha, *J. Opt. Soc. Am. B* **2019**, *36*, 684–689.

[8] a) I. Stassen, N. Burtch, A. Talin, P. Falcaro, M. Allendorf, R. Ameloot, *Chem. Soc. Rev.* **2017**, *46*, 3185–3241; b) P. Falcaro, R. Ricco, C. M. Doherty, K. Liang, A. J. Hill, M. J. Styles, *Chem. Soc. Rev.* **2014**, *43*, 5513–5560; c) O. M. Yaghi, M. J. Kalmutzki, C. S. Diercks, *Introduction to Reticular Chemistry: Metal-Organic Frameworks and Covalent Organic Frameworks*, Wiley, **2019**; d) S. Kitagawa, *Chem. Soc. Rev.* **2014**, *43*, 5415–5418.
[9] a) L. Heinke, C. Wöll, *Adv. Mater.* **2019**, *31*, 1806324; b) O. Shekhah, H. Wang, S. Kowarik, F. Schreiber, M. Paulus, M. Tolan, C. Sternemann, F. Evers, D. Zacher, R. A. Fischer, C. Wöll, *J. Am. Chem. Soc.* **2007**, *129*, 15118–15119.
[10] K. Zhan, Y. Jiang, P. Qin, Y. Chen, L. Heinke, *Advanced Materials Interfaces* **2023**, *10*, 2300329.
[11] Z.-G. Gu, S. Grosjean, S. Bräse, C. Wöll, L. Heinke, *Chem. Commun.* **2015**, *51*, 8998–9001.
[12] S. S.-Y. Chui, S. M.-F. Lo, J. P. Charmant, A. G. Orpen, I. D. Williams, *Science* **1999**, *283*, 1148–1150.
[13] S. Okur, P. Qin, A. Chandresh, C. Li, Z. Zhang, U. Lemmer, L. Heinke, *Angew. Chem. Int. Ed.* **2021**, *60*, 3566–3571.
[14] A. E. Rodrigues, I. Nogueira, R. P. Faria, *Molecules* **2021**, *26*, 3095.
[15] S. Hurrle, S. Friebe, J. Wohlgemuth, C. Wöll, J. Caro, L. Heinke, *Chem. Eur. J.* **2017**, *23*, 2294–2298.
[16] Z.-G. Gu, A. Pfriem, S. Hamsch, H. Breitwieser, J. Wohlgemuth, L. Heinke, H. Gliemann, C. Wöll, *Microporous Mesoporous Mater.* **2015**, *211*, 82–87.
[17] J. N'Guimbi, C. Berro, I. Mokbel, E. Rauzy, J. Jose, *Fluid Phase Equilib.* **1999**, *162*, 143–158.
[18] H. T. Archana, D. Sachin, *Int. J. Comput. Appl.* **2015**, *122*, 4–8.
[19] a) P. Qin, B. A. Day, S. Okur, C. Li, A. Chandresh, C. E. Wilmer, L. Heinke, *ACS Sens.* **2022**, *7*, 1666–1675. ; b) K. Zhan, P. Qin, Y. Jiang, Y. Chen, L. Heinke, *Sens. Actuators B* **2023**, *393*, 134271.

Manuscript received: February 27, 2024
Accepted manuscript online: April 16, 2024
Version of record online: ■■, ■■

# RESEARCH ARTICLE

A colorimetric sensor array made of Fabry-Pérot films based on different chiral metal-organic frameworks is presented. The color changes as response to analyte vapor molecules. The sensors respond enantioselectively for chiral vapor molecules. In combination with a common smartphone camera, the sensor array is used as simple and cost-efficient system to detect and identify a large number of perfume samples.

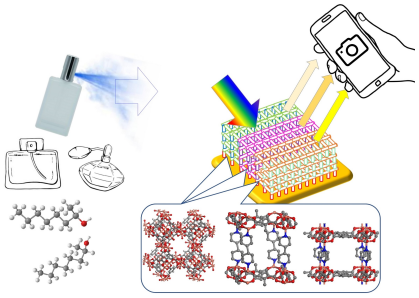

*Dr. K. Zhan, Dr. A. B. Kanj, Priv.-Doz. Dr. L. Heinke**

1 – 8

**Classification and Identification of Perfume Scents by an Enantioselective Colorimetric Sensor Array of Chiral Metal-Organic-Framework-Based Fabry-Pérot Films**